



**HAL**  
open science

# Prediction by DFT and Docking Calculations of a Series of Hypothetical 3d Transition Element Isostructural Complexes [M(hfac) 2 (TTF) 2 ]: A Comparative Study

Samira Zeroual, Saliha Belhouchat, Saad Bouchekioua, Rafik Menacer,  
Oussama Khaoua, Noura Benbellat, Henry Chermette

## ► To cite this version:

Samira Zeroual, Saliha Belhouchat, Saad Bouchekioua, Rafik Menacer, Oussama Khaoua, et al.. Prediction by DFT and Docking Calculations of a Series of Hypothetical 3d Transition Element Isostructural Complexes [M(hfac) 2 (TTF) 2 ]: A Comparative Study. *ChemistrySelect*, 2024, 9 (38), 10.1002/slct.202403632 . hal-04798942

**HAL Id: hal-04798942**

**<https://hal.science/hal-04798942v1>**

Submitted on 22 Nov 2024

**HAL** is a multi-disciplinary open access archive for the deposit and dissemination of scientific research documents, whether they are published or not. The documents may come from teaching and research institutions in France or abroad, or from public or private research centers.

L'archive ouverte pluridisciplinaire **HAL**, est destinée au dépôt et à la diffusion de documents scientifiques de niveau recherche, publiés ou non, émanant des établissements d'enseignement et de recherche français ou étrangers, des laboratoires publics ou privés.

## Prediction by DFT and Docking calculations of a series of hypothetical 3d transition element isostructural complexes $[M(\text{hfac})_2(\text{TTF})_2]$ , a comparative study.

Samira ZEROUAL<sup>a</sup>, Saliha BELHOUCHEAT<sup>a</sup>, Saad BOUCHEKIOUA<sup>b</sup>, Rafik MENACER<sup>b,c</sup>, Oussama KHAOUA<sup>a</sup>, Noura BENBELLAT<sup>a</sup> and Henry CHERMETTE<sup>d,\*</sup>

<sup>a</sup>Laboratoire de Chimie des Matériaux et des Vivants: Activité & Réactivité(LCMVAR), Département chimie, Faculté des Sciences de la Matière, Université de Batna 1, Algeria.

<sup>b</sup>Centre de recherche en Sciences Pharmaceutiques (CRSP), Constantine, Algérie.

<sup>c</sup>Centre de Recherche Scientifique et Technique en Analyses Physico-Chimiques (CRAPC), Tipaza, Algeria

<sup>d</sup> Institut des Sciences Analytiques de Lyon, UMR 5280 CNRS, Université Claude Bernard Lyon 1, F-69622 VILLEURBANNE Cedex, France.

e-mails: samira.zeroual@univ-batna.dz, henry.chermette@univ-lyon1.fr

### Abstract.

The aim of this study is to predict and compare the structural, electronic, conductivity and biological properties of a series of 3d transition element complexes with those of the previously studied iso structural copper complex  $[\text{Cu}(\text{hfac})_2(\text{TTF})_2][\text{PF}_6]_2$  (TTF: Tetrathiafulvalene, hfac: hexafluoroacetylacetonate). Because transition metals hold open electronic shells, All possible spin states for all compounds **divalent** have to be considered in order to determine the most stable configurations. These configurations are those corresponding to the highest spin state (5 for Mn, 4 for Fe, 3 for Co, 2 for Ni, 1 for Cu and 0 for Zn), However, the configurations with the smallest gap are Mn (3) and Co (1), suggesting that these are the most conductive complexes.

A significant metal-ligand charge transfer is observed for both Mn and Co complexes. Antifungal (CYP121 (PDB: 2IJ7) and CYP51 (PDB: 1EA1)) and antibacterial (*E. coli* (PDB: 1KZN)) of the compounds studied were evaluated by molecular docking; the results obtained reveal that the following complexes show significant activity: Zn(hfac)<sub>2</sub>(TTF)<sub>2</sub>[PF6]<sub>2</sub> (-8.9 kcal/mol), Ni(hfac)<sub>2</sub>(TTF)<sub>2</sub>[PF6]<sub>2</sub> (-7.8 kcal/mol) and Cu(hfac)<sub>2</sub>(TTF)<sub>2</sub>[PF6]<sub>2</sub> (-8.2 kcal/mol).

## Introduction

Transition elements form many coordination compounds thanks to the presence of the incomplete d-orbital shell [1]. In complexes, the metal cations hold empty s orbitals, and, in part, some d orbitals capable of receiving electron doublets from ligands. All transition elements have several properties in common: they are all metals, relatively hard, have high melting and boiling temperatures, conduct heat and electricity. They have low electronegativity; hence good reducing properties. Finally, they can form ions in different oxidation states, due to their electronic structure. Transition elements and their compounds very often exhibit catalytic properties [2, 3].

Coordination complexes have been the subject of a great deal of work over the last few decades [4-7], and in particular they have experienced astonishing development due to their numerous applications in catalysis [8], biology [9] and the pharmaceutical industry [10].

The history of conductive organic materials goes back to 1954, when H. Akamatu reported that perylene bromide is highly conductive [11]. Following this initial discovery, in 1960, a series of conducting salts were synthesized from the organic acceptor tetracyanoquinodimethane (TCNQ) [12]. In 1962, Wudl et al. described the synthesis of an electron- $\pi$  donor molecule (TTF: tetrathiafulvalene) [13], soon followed by the first conductivity measurements of the TTF chloride salt [14]. The fundamental step was taken in 1973 by Cowan et al [15] with the formation of the first true "organometallic" charge transfer complex (CTC) conductor by combining the acceptor TCNQ and the organic donor TTF: TTF-TCNQ (tetrathiafulvalene-tetracyanoquinodimethane) [16-18].

This discovery encouraged researchers to synthesize numerous TTF-TCNQ-type organic conductive materials with high conductivity at room temperature, such as (TSF-TCNQ)[19], (HMTSF-TCNQ) [20] and (HMTSF-2, 5-DMTCNQ) [21]. Unfortunately, at low temperatures, most CTCs undergo a metal-insulator transition, known as the Peierls transition, due to the structural deformation known to occur in one-dimensional systems. Note that in the TTF-TCNQ compound, a structural and electronic transition takes place below 60 K, leading to semiconducting behavior;

In 1992, the synthesis of the first molecular system with multiple properties suitable for electrical and magnetic applications mobilized chemists, physicists and theorists. This first molecular conductor incorporating paramagnetic ions demonstrated a stable metallic state and ferromagnetic interaction between Cu (II) ions: (BEDTTTF)<sub>3</sub>CuCl<sub>4</sub>.H<sub>2</sub>O. In 2003, Ouahab et al [22] developed a new series of organic/inorganic hybrid materials involving coordination between a paramagnetic transition metal and a TTF derivative, where the ligands are either in the trans or cis position. Their oxidation by electrocrystallization enabled us to isolate salts with radical cations of the formula [M(hfac)<sub>2</sub>(TTF-CH=CH-py)<sub>2</sub>](PF<sub>6</sub>)<sub>n</sub>. hfac = hexafluoroacetylacetonate, M = Cu (II), Mn(II) which are either fully oxidized (n = 2) or mixed valence (n = 1). The magnetic properties of the Cu(hfac)<sub>2</sub>(TTF-CH=CH-py)<sub>2</sub> complex, measured from 5 to 300 K, reveal paramagnetic behaviour corresponding to the isolated spin S = 1/2 of Cu (II).

The main factors known to influence the conductivity of this type of material are structural and electronic. Our work therefore aims to elucidate, via theoretical approaches, these two factors and also the effect of changing the central metal on the various properties of the compounds in question [23].

DFT and TDDFT calculations were carried out using the B3LYP/6-311G(d,p) level of theory to analyze the frontier orbitals, molecular electrostatic potentials and vertical excitation energies of the title compounds. Atoms In Molecules (AIM), Energy Decomposition Analysis (EDA), Molecular Electrostatic Potential (MEP), and Non-Covalent Interactions (NCI plot) are reliable methods we have

used to identify and examine the nature of intra- and intermolecular bonding in our compounds. In addition, molecular docking studies have enabled a theoretical assessment of likely biological activities.

## Methods and Results

As mentioned previously, this study is a follow-up and comparative to a first one concerning the  $[\text{Cu}(\text{hfac})_2(\text{TTF})_2] [\text{PF}_6]_2$  complex [23], and accordingly, all the calculations were carried out with the same theoretical protocol. Density Functional Theory (DFT) was used using Generalized Gradient Approximation (GGA), including scalar relativistic corrections through Zero-Order Regular Approximation (ZORA) [24]. These DFT/ZORA calculations were performed with the ADF (Density Functional Theory) code [25]. We used the same GGA (Generalized Gradient Approximation) functional: PBE (Perdew-Burke-Ernzerhof) [26, 27], and the TZP (Triple Zeta + Polarization) basis set. The bonding characteristics of the compounds are analyzed using Bader's AIM [28] theory and carried out using the DGrid/Basin [29] program. TD-DFT [30] was used to obtain the absorption wavelengths, oscillation force, gap energies, major contribution and charge transfer character. All calculations were carried out in the gas phase. All possible spin states for each metal have been taken into consideration.

Finally, molecular docking studies were carried out using Autodock 4.1 package, in order to examine the mechanism of actions and the binding mode of the complex, towards the target proteins [31- 35].

### 1. DFT Study of Transition Metal Complexes Based on TTF Ligand

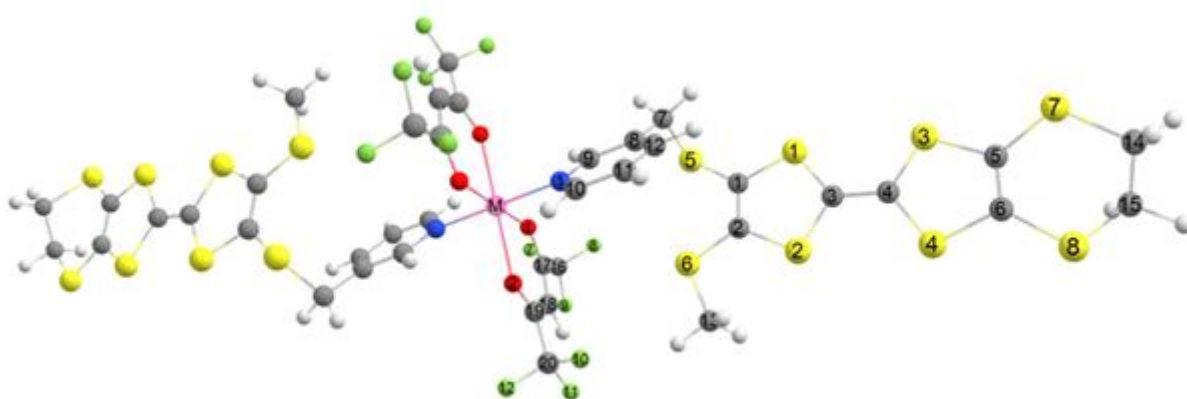
The transition metal coordination complexes with the **4-methylthio-5-(3-picolythio)-4,5-dimethylenedithiotétrathiafulvalene** ligand of formula  $\text{M}(\text{hfac})_2(\text{TTF})_2$  (where: **M = Mn, Fe, Co, Ni, Cu and Zn**) have been studied to predict the properties of the corresponding complexes. The DFT results on the M-complexes behave as a regular octahedral. The EDA analysis is employed to interpret the nature of the metal–ligand bond in the complexes. Photophysical properties of the coordination complexes have been studied by time dependent density functional theory (TD-DFT) calculations to identify the nature of the different electronic transitions according to their molecular orbital localization and to reproduce the absorption spectrum.

#### 1.1. Structural Analysis of the Organometallic Complexes

At this level, we have undertaken a theoretical study of the real compound  $[M(\text{hfac})_2(\text{TTF})_2]$  (with  $M = \text{Cu}$ ) and hypothetical ones ( $M = \text{Mn}, \text{Fe}, \text{Co}, \text{Ni}$  and  $\text{Zn}$ ) in  $C_i$  symmetry. The goal of this series is to see how the ligand interaction changes along the period.

The optimized structure of the investigated organometallic complexes for each metal ion is depicted in **Fig.1**, while the geometry parameters are represented in the **Fig. 2** highlights the variation of them along the series.

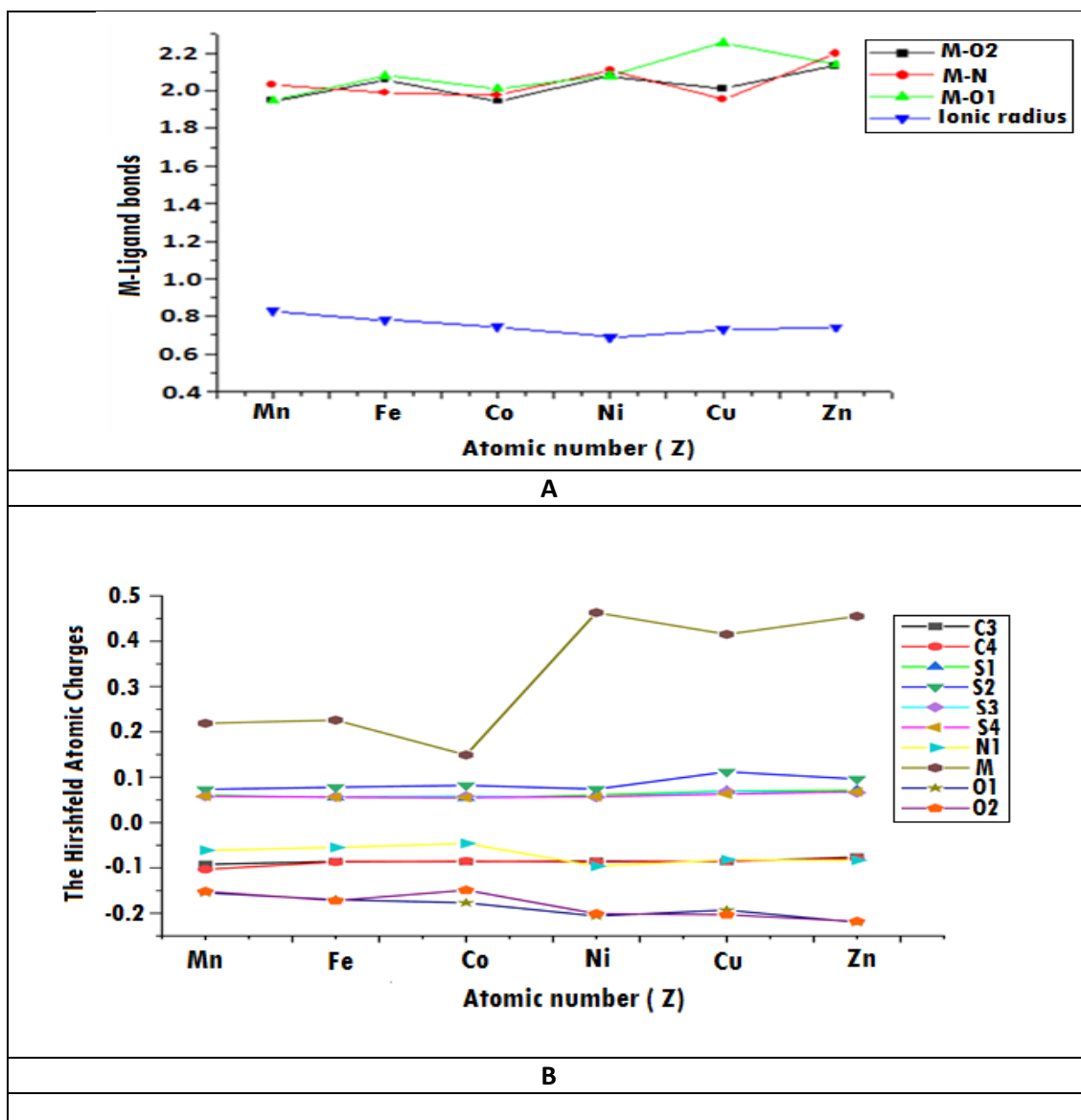
For all  $[M(\text{hfac})_2(\text{TTF})_2]$  complexes the  $M$  metal atom is at the center of inversion in a distorted octahedral coordination geometry.  $M$  is coordinated by four oxygen atoms from the bidentate  $\text{hfac}$  ligands in the basal plane and two nitrogen atoms from the  $L$   $\text{TTF}$  ligands in the apical positions.



**Fig. 1** The optimized structure for organometallic complex  $[M(\text{hfac})_2(\text{TTF})_2]$  (with  $M = \text{Mn}, \text{Fe}, \text{Co}, \text{Ni}, \text{Cu}, \text{Zn}$ ).

It is remarkable that the  $[\text{Zn}(\text{hfac})_2(\text{TTF})_2]$  (**6**) has the longest average C3-C4 bond length at 1.371 Å and the shortest value at 1.349 Å is found in  $[\text{Cu}(\text{hfac})_2(\text{TTF})_2]$  (**5**). The computed distances of metal-oxygen coordination bonds M-O1 and M-O2 vary in the ranges (1.941 Å [Fe] - 2.201 Å [Co]), and (1.939 Å [Fe] - 2.254 Å [Cu]). Also, the longest average M-N distance is 2.198 Å and the shortest value is 1.953 Å, respectively, in **6** and **5** metal complexes. As a result, the M-N values are shorter in the order of  $\text{Cu} < \text{Co} < \text{Fe} < \text{Mn} < \text{Ni} < \text{Zn}$ . There is little variation of the M-N bond lengths for different metal complexes. One can observe that the changes on the bond distances is small among the studied compounds. The optimized O1-M-O1, N1-M-N1 and O2-M-O2 bond angles in all metal complexes are equal to 180° and

O–M–N bond angles vary, not significantly, from 89° to 91°. The net atomic charges of these complexes are obtained using the Hirshfeld analysis. The charges on the metals are (+0.219), (+0.148), (+0.149), (+0.463), (+0.415) and (+0.455), from Mn to Zn respectively.



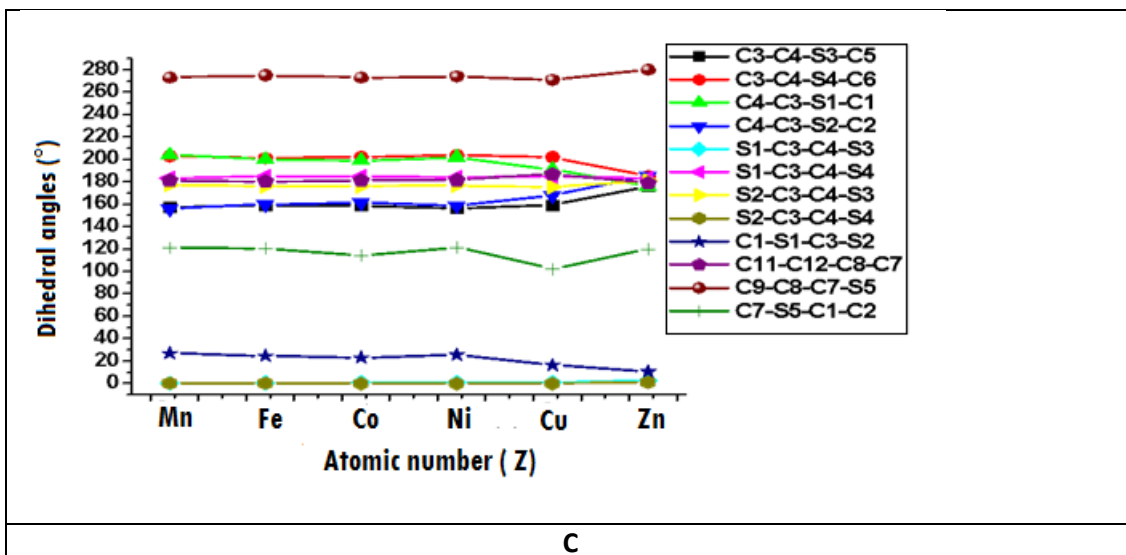


**Fig. 2 Graphical representation of the evolution of A: bonds length and ionic radius[36], B: atomic charge depending on atomic number Z and C: dihedral angles**

The complexes of Mn, Fe, Ni and Zn present regular octahedral geometries, however the two complexes based on Co and Cu are deformed (pseudo-octahedrons), this is due to the Jahn-Teller effect which is responsible for the distortion of the complex having a degenerate fundamental electronic level.

The bond length in the apical position (between the metal and the nitrogen) decreases with the increase in the atomic number Z with the exception of Ni and Zn. The metal charge increases with Z with the exception of Co. In general, for odd Z atomic numbers, the charge of the metal decreases when the charge of the coordinated atoms increases, and the reverse is obtained for the even Zn **Fig 2 C**. In addition, the charge carried by the metal [Ni] is the highest so this compound shows a stronger ionic bond. **It is worth to notice that the MO1 and MO2 follow the Irving-Williams series (Fe being slightly off), whereas for the Jahn-Teller distorted complexes, the M-O1 does not follow the rule (especially the copper complex), underlining the stabilizing role of that bond, since M-N and M-O2 keep similar lengths.**

## 1.2. Molecular Orbital Analysis

The frontier molecular orbitals (FMOs) play a crucial role to determine the electronic properties of a chemical system. The selected molecular orbitals FMOs compositions in addition to the energy gaps  $\Delta E$

gap of the studied complexes are tabulated in **Table 1**, where the nodal properties of SOMOs and LUMOs of  $\alpha$ -spin and the molecular orbital diagrams are displayed in **Figs. 3 and 4**.

All calculations are performed on neutral complexes, which can exist with different spin states;

1, 3, or 5 SOMOs for the complex with Mn. For the Co complex, we should have 1, or 3 SOMOs, for Cu, we have one SOMO. For Fe, we should have zero, or 2, or 4 SOMOs, and for Ni, we should have **0** or 2 SOMOs. In the case of **0**, we're talking about a HOMO.

Table 6 shows the different spin state possibilities for each complex and, their Total Energies (ET) and the corresponding gap.

All calculations are in the unrestricted formalism, except for the Zn complex which is known by its diamagnetic state, and Fe, which can be either para- or diamagnetic.

The analysis of the distribution and the spin of the electrons confirm that the other complexes (with Mn, Co, Ni and Cu) are paramagnetic.

**Table 1.** The different spin state possibilities for each complex and their Total Energies

Central metal	Spin states with Total Energies (eV) and Gap energies (bold italic)					
	0	1	2	3	4	5
Mn		-617.301		-617.731		-617.901
		<b><i>1.088</i></b>		<b><i>0.243</i></b>		<b><i>1.112</i></b>
Fe	-616.660		-615.994		-617.031	
	<b><i>1.036</i></b>		<b><i>1.026</i></b>		<b><i>1.430</i></b>	
Co		-615.095		-615.633		
		<b><i>0.894</i></b>		<b><i>1.401</i></b>		
Ni			-612.445			
			<b><i>1.233</i></b>			
Cu		-598.590				
		<b><i>1.141</i></b>				
Zn	-608.932					
	<b><i>1.154</i></b>					

The most stable compounds have the largest gap (maximum hardness principle) and the maximum spin multiplicity. The energy gap between the different spin states is small, so configuration changes are possible.

Mn (3) has the smallest gap (0.2 eV) followed by Co (1) with 0.8 eV. The other compounds have a similar gap with a value around 1 eV.

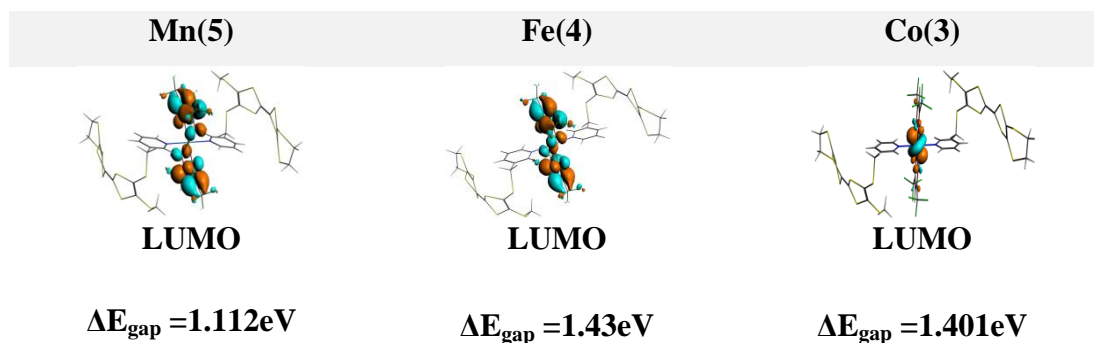
**Table 2.** The HOMO/SOMO, LUMO, and the  $\Delta E$  gap (in eV) calculated at the PBE / TZP level for the most stable configurations (Mn (5), Fe (4), Co (3), Ni (2), Cu (1) and Zn (0)).

FOMs	Mn (5)		Fe (4)		Co (3)		Ni (2)		Cu (1)		Zn (0)	
	SOMO	LUMO	HOMO	LUMO								
E (eV)	-4.525	-3.413	-4.803	-3.373	-4.794	-4.341	-4.482	-3.249	-4.477	-3.335	-4.370	-3.216
M %	63.40	0	0	0	1.67	88.07	0	0	0	0	0	0
O %	22.26	28.26	0	26.98	0	1.80	0	27.61	0	27.47	9.12	0
N %	1.37	0	0	0	0	0	0	0	0	0	0	0
$\Delta E_{\text{gap}}$	1.112		1.026		1.401		1.233		1.141		1.154	

the percentage of the contribution of the metal in the HOMO and the LUMO orbitals gives us a very good insight into the ability of this metal to be a good catalyst [37].

According to our results, it appears that Mn, Ni, Cu and Zn transition metals may exhibit good catalytic activity, while, the others complexes are good conductors.

The energy gap is closely associated with the reactivity and stability of a molecule and shows its nature with  $\Delta E$  of the studied complexes varying between 1.026 eV for complex Fe(4) more reactive and 1.4 eV for complex Co (4) less reactive (**Table 2**) than the other complexes, so that an electron fluctuation between these orbitals may occur. As well as the energy gap of  $\alpha$ -spin for these compounds increases of the order of Fe < Mn < Cu < Zn < Ni < Co



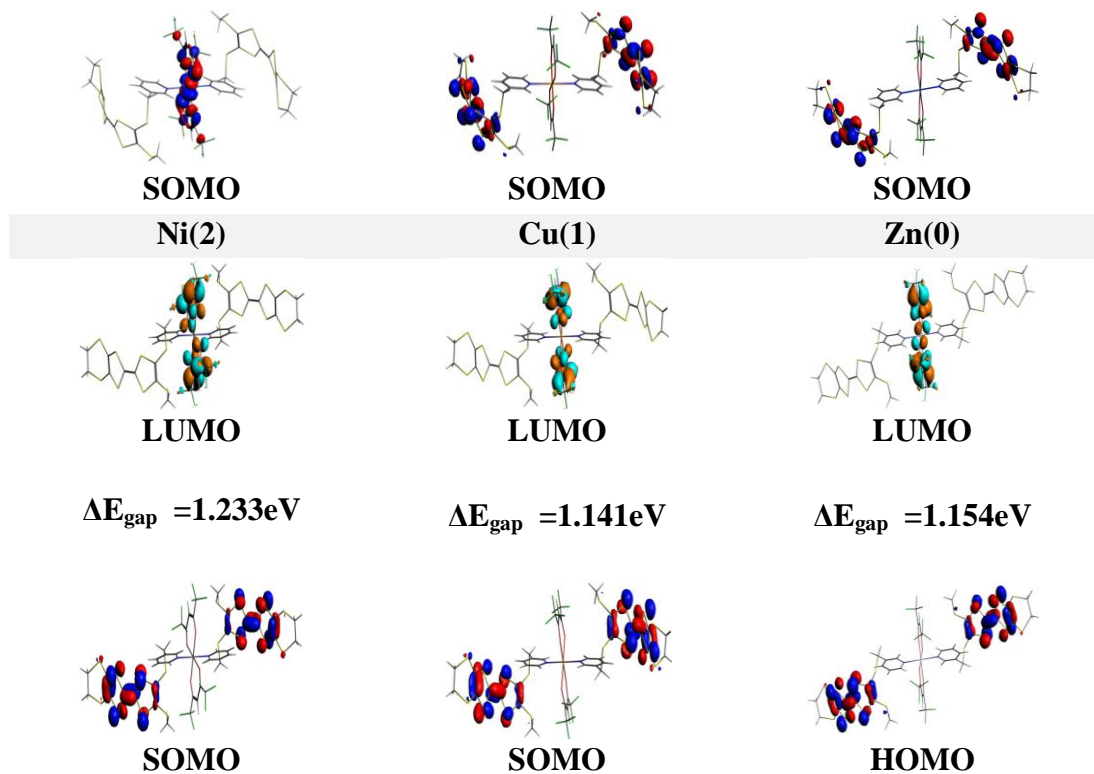


**Fig. 3** Frontier molecular orbitals HOMO/ SOMOs and LUMOs of the most stable configurations (Mn (5), Fe (4), Co (3), Ni (2), Cu (1) and Zn (0), obtained at PBE / TZP level.

For Fe, Ni and Cu complexes, the electron density of the SOMO is localized mainly on the TTF moiety, whereas the LUMO is localized only on the bidentate hfac. In the Zn complex, the HOMO is localized on all atoms of TTF, whereas the LUMO is focused only in the two hfac parts. In Co complex, the SOMO localized on TTF moiety with a small contribution on Co ion (1.67%), but the LUMO is mainly distributed on the metal with a percentage of metal contribution 88.07% with a weak participation of the O atoms with 1.8 % , which gives rise to the possibility of metal- to- ligand charge transfer.

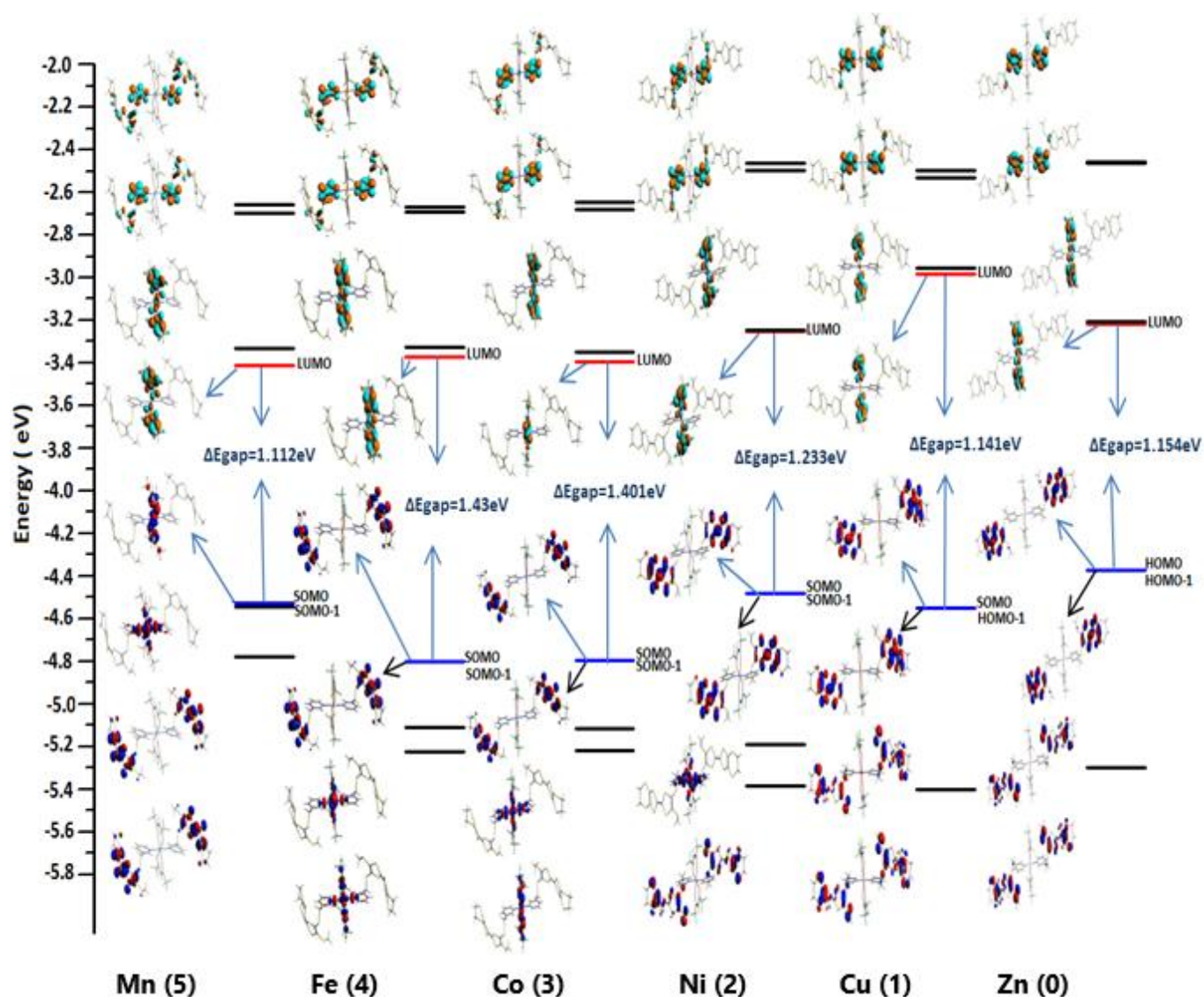


**Figure. 4** Frontier molecular diagrams for the most stable configurations (Mn (5), Fe (4), Co (3), Ni (2), Cu (1) and Zn (0) metal complexes obtained at PBE/TZP level of theory.

For the Mn complex the SOMO is localized mainly on the metal with a percentage of metal contribution 63.4% which indicates a metallic character with a weak participation of the N atom of percentage 1.37%, while the LUMO is mainly localized on metal with a metallic percentage of 61.05%. The SOMO of the Fe complex exhibits a weak metallic character (2.85%) and ligand of (87.55%), while the LUMO is localized on the atoms of hfac ligands.

The degeneracy of the orbitals HOMO/SOMO and HOMO-1/SOMO-1 (until even SOMO-2 for the complexes of Cu and Zn) on the one hand, and of the LUMO/LUMO+1 on the other hand, is in favor of the conductive nature of these complexes. The complexes with Mn, Ni, Cu and Zn have a ligand-type HOMO/SOMO, and a metal-type LUMO, and this allows the electron to pass from one side of the complex to the other. In the two complexes with Co and Fe, however, the two frontier orbitals are of the same type (located on the ligand).

Changing of HOMO/LUMO energy gap value leads to a change in the conductivity of the studied compounds. The well-known relationship between the energy gap and conductivity is expressed by the following equation [38] :  $\sigma = e^{-E/2k_B T}$

Where  $\sigma$  is the electrical conductivity,  $k_B$  is the Boltzmann constant and  $T$  is Kelvin temperature. As the equation shows, the conductivity increases as the energy gap decreases. Thus, the conductivity of complexes with Mn, Fe and Co is the highest because they have smaller energy gaps.

### 1.3. Energy Decomposition Analysis

Energy decomposition analysis have been done to emphasize the nature of the considered chemical bonds. The total bonding energy is decomposed into three terms,  $\Delta E_{\text{Pauli}}$ ,  $\Delta E_{\text{elec}}$ , and  $\Delta E_{\text{orb}}$ , which correspond respectively to the repulsive, electrostatic and orbital interactions between the fragments. For performing EDA analysis, we considered the TTF ligand L is as one fragment to study its binding energy with the M metal and the (hfac) part as the other fragment. The bonding energies and the type of the corresponding bonds between pair of fragments reported in **Table 3**.

**Table 3.** Energy decomposition analysis (EDA) into Pauli, electrostatic energies, and orbital interactions of M-N and M-O (M= (Mn (5), Fe (4), Co (3), Ni (2), Cu (1) and Zn (0)) at BLYP/TZP level.

Bond	Energy parameters	Complexes					
		Mn (5)	Fe (4)	Co (3)	Ni (2)	Cu (1)	Zn (0)
M-N	$\Delta E_{\text{Pauli}}$	12.61	12.62	12.35	7.46	7.2	4.79
	$\Delta E_{\text{elecst}}$	-8.37	-9.04	-8.79	-5.82	-6.2	-4.88
	$\Delta E_{\text{orb}}$	-8.98	-11.29	-7.23	-4.08	-3.3	-2.15
	$\Delta E_{\text{int}}$	-4.74	-7.71	-3.67	-2.40	-2.3	-2.24

	<b>% covalent</b>	51.76	55.53	45.13	41.21	34.7	30.58
	<b>% ionic</b>	48.24	44.47	54.87	58.79	65.3	69.42
<b>M-O</b>	$\Delta E_{\text{Pauli}}$	27.83		16.92	15.82	8.12	15.97
	$\Delta E_{\text{elecst}}$	-14.24		-8.64	-8.89	-5.02	-9.1
	$\Delta E_{\text{orb}}$	27.84		-17.70	-14.77	-9.97	-16.22
	$\Delta E_{\text{int}}$	-14.25		-9.42	-7.85	-6.87	-9.35
	<b>% covalent</b>	66.16		67.20	62.43	66.51	64.06
	<b>% ionic</b>	33.84		32.8	37.57	33.49	35.94

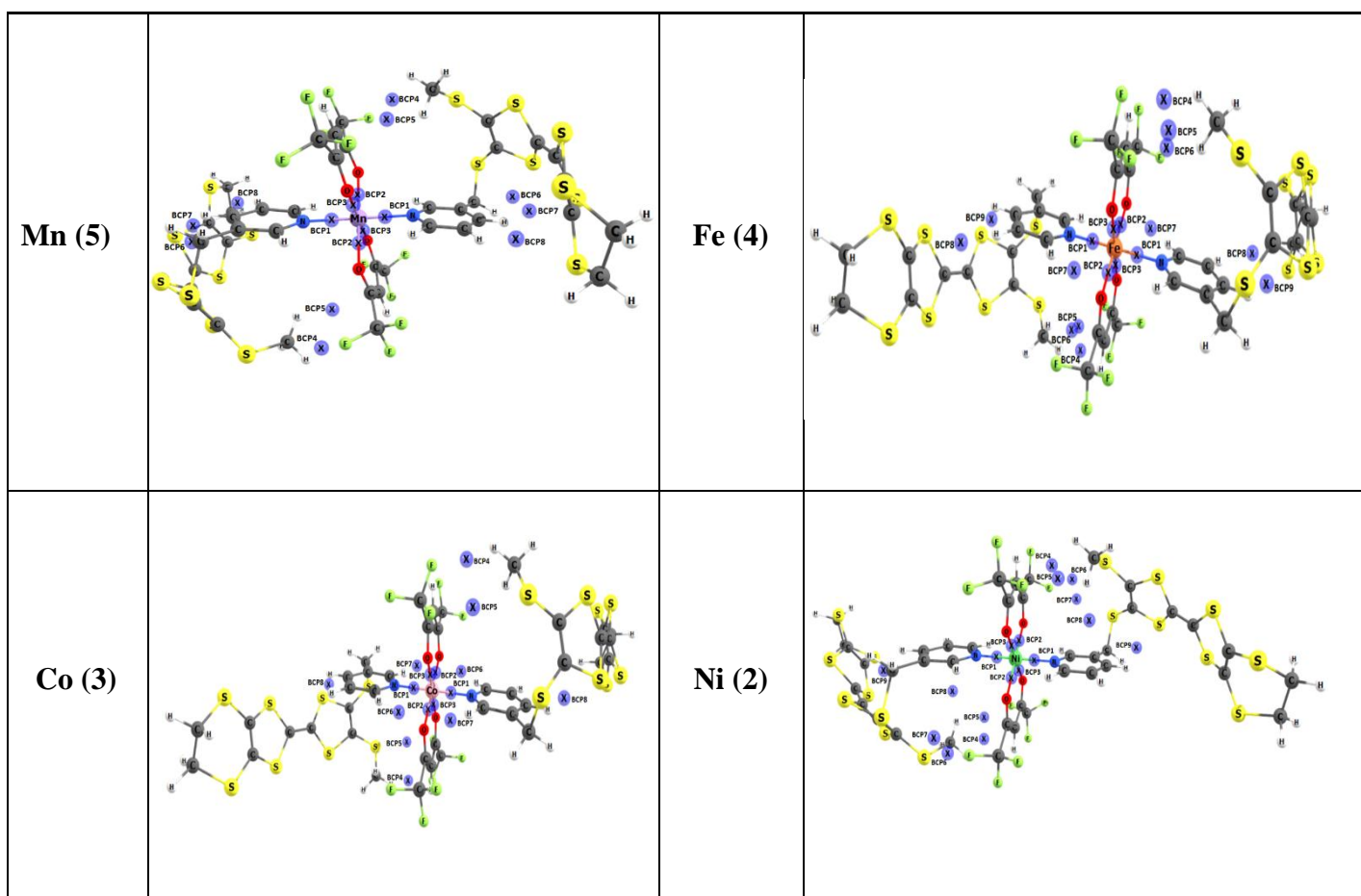
In the case of the M-N bonds the major contributions on the total bonding energy is the Pauli repulsion rather than electrostatic energy  $\Delta E_{\text{elec}}$  and orbital energy ( $\Delta E_{\text{orb}}$ ) for all the complexes. Then, the contribution of  $\Delta E_{\text{orb}}$  is less than the  $\Delta E_{\text{elec}}$  for Co, Ni, Cu and Zn metals. The % contribution of the electrostatic interaction (ionic character) is the major interaction in Co, Ni, Cu and Zn complexes.  $\Delta E_{\text{orb}}$  can be considered as an estimation of the covalent contributions to the attractive interactions, whereas in the case of the M-O bonds in the complex  $[M(\text{hfac})_2 (\text{TTF})_2]$  the covalent contribution is dominant in all complexes.

#### 1.4. Topological Analysis (AIM)

The analysis by the AIM method that we applied to our compounds to get significant information on the Metal-L chemical bonds, in particular the weak non-covalent interactions. The results of this analysis clearly indicate the existence of six critical points (BCPs) metal- ligand interactions of the coordination of the metal with pyridine and hfac bidentate units and the intramolecular interactions. The number of existing intramolecular BCPs differs according to the complexes. For the [Mn, Co, Cu and Zn] we observed five non covalent intramolecular BCPs, while in [Fe and Ni], we observe six BCPs as shown in **Fig. 19**. Chemical bonds can be characterized and classified based on electron properties and energy densities at the BCP level. In this work, the calculation of topological parameters such as the electron

density  $\rho(r)$ , its Laplacian  $\nabla^2\rho(r)$ , and the energy density  $H$ , at the BCPs of the M-L bond and noncovalent intramolecular bonds for the considered systems are provided in **Table SI (Supplementary)**.

The analysis of topological parameters suggested a positive value of both  $\nabla^2\rho(r)$ , and  $H(r)$  with a very small value of  $\rho(r)$  for the non-covalent bonds whereas a positive value of  $\nabla^2\rho(r)$ , and a negative value of  $H(r)$  with moderate  $\rho(r)$  correspond to a bond which is partially covalent in nature. The larger Value of  $\rho(r)$  BCPs are mainly due to the M – N bonds signifying that they are the stronger than M-O and increases in the order Zn < Ni < Mn < Fe < Cu. Other parameters of the theory AIM prove the existence of weak intramolecular hydrogen bond F ... H-C and S ... H-C, with a low value of electron density, and a positive Laplacian, the ratio  $|V|/G < 1$ , with  $H(r) > 0$ , indicating mainly an electrostatic nature.



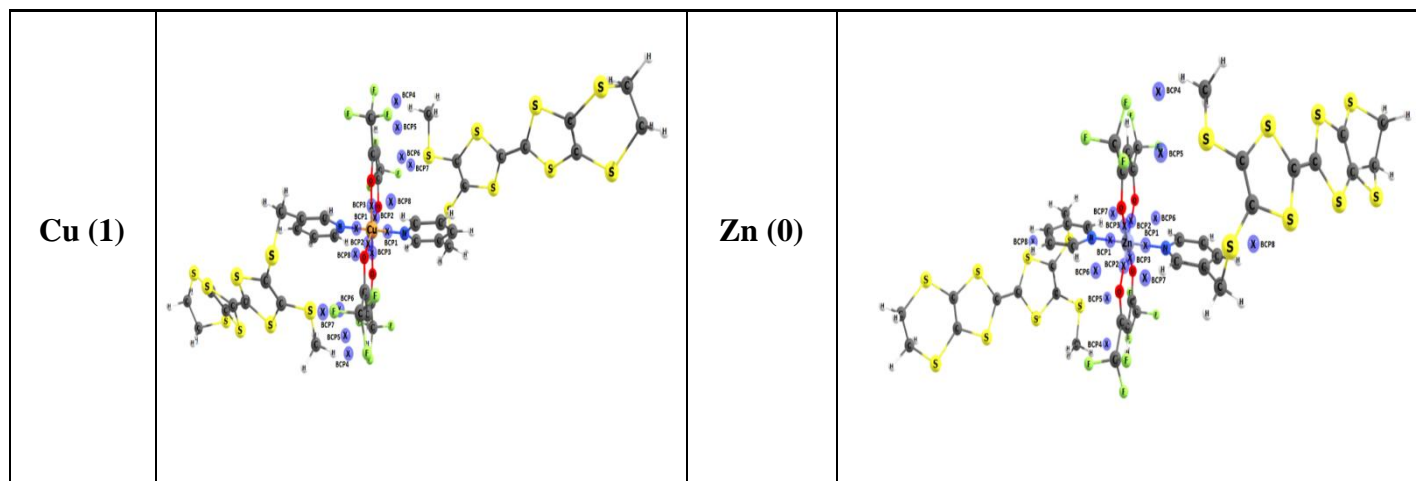


**Fig. 5.** Molecular graph showing magenta Bond Critical Points (BCPs) of  $[M(\text{hfac})_2\text{TTF}_2]$  (**Mn (5)**, **Fe (4)**, **Co (3)**, **Ni (2)**, **Cu (1)** and **Zn (0)**)

### 1.5. The Electronic Absorption Spectra

The electronic properties of the transition metals (Cu, Co, Mn, Ni, Zn and Fe) having TTF ligands are investigated using the TD-DFT method. The identification of the nature of the different electronic transitions is based on the coefficients of molecular orbitals. Theoretical calculations on the shape and the position of such transition are identified as MLCT, ILCT or LMCT charge transfer.

The electronic spectra calculated at the PBE / TZP level of the optimized complexes are presented in **Fig.6** and the main electronic transitions, the wavelengths, the percentage of the dominant contributions of the electronic excitations, are reported in **Table S2**. These complexes absorb in the same wavelength range, with a significant shift of the maximum wavelength going from Mn to Zn.

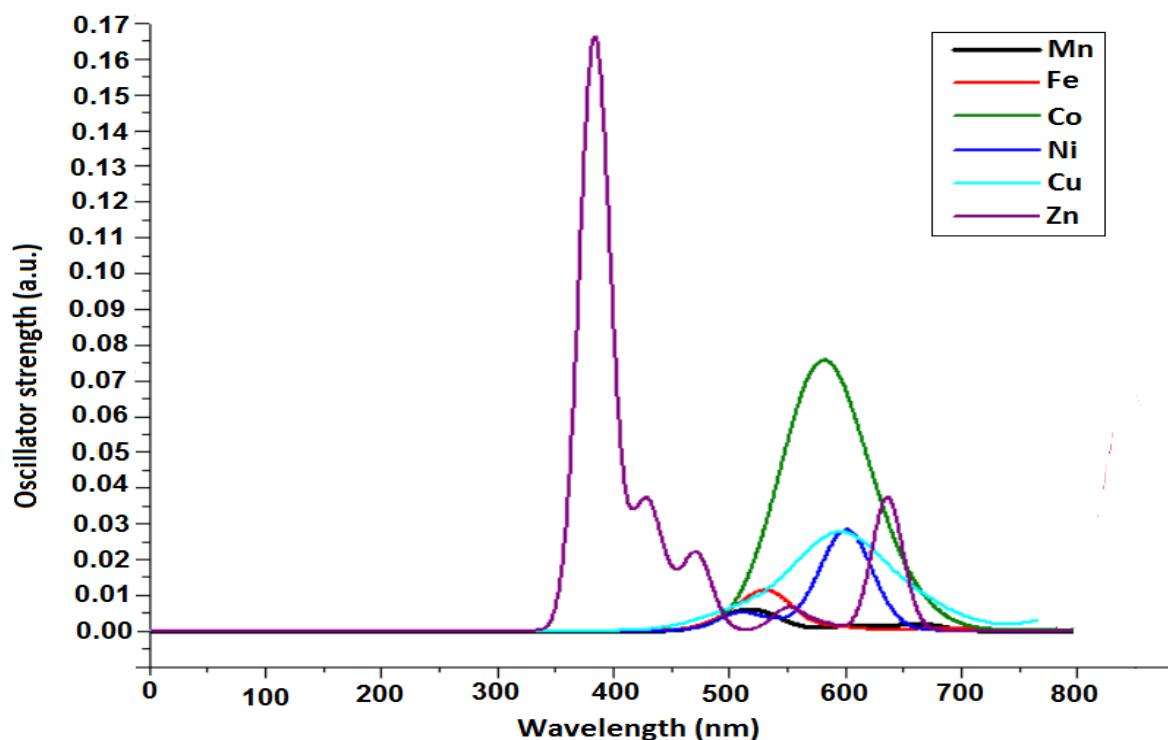


**Fig.6** TD-DFT theoretical electronic spectra of the metal complexes [Mn, Fe, Co, Ni, Cu and Zn] obtained at DFT/PBE level.

The TD-DFT calculation of the Mn complex presents three bands, the first absorption band at 519 nm for the  $\beta$ -spin due to electronic transition HOMO-5  $\rightarrow$  LUMO (99.7%) and at 516 nm consisting of two transitions (SOMO-1 $\rightarrow$ LUMO+4) for the  $\beta$ -spin and (SOMO-3 $\rightarrow$ LUMO+4) for the  $\alpha$ -spin, of nature 55.8% (LMCT) and 20.8% (ILCT) respectively. The second absorption band arising at 612 nm correspond to MLCT transfer transition from SOMO $\rightarrow$  LUMO+4 (99.9%) for the  $\alpha$ -spin. The third

absorption band located at 664 nm for the  $\alpha$ -spin consisted the transition SOMO $\rightarrow$  LUMO+2 (99.9%) of the character MLCT. (**Figure S1** ). The electronic transitions for the Mn complex are the MLCT, LMCT and ILCT types.

The Fe complex mainly shows **two** absorption bands at 529nm and 685nm. The band 529nm is associated with two transitions SOMO $\rightarrow$  LUMO+3 (15.6%) and SOMO-2 $\rightarrow$  LUMO+5 (63.9%) respectively of type ILCT for the  $\alpha$ -spin and  $\beta$ -spin. At 685nm band correspond to MLCT electronic transition from SOMO-2 $\rightarrow$  LUMO+1 (98.6%).

The theoretical absorption spectrum of Co complex presents tow absorption bands at 544nm, and 642nm .The first contain two transitions (SOMO-1 $\rightarrow$ LUMO+4) (27.7%) and (SOMO $\rightarrow$ LUMO+4) (19.7%) of same type ILCT for the  $\alpha$ -spin and tow transition (SOMO  $\rightarrow$ LUMO + 6) (41.8%) and (SOMO  $\rightarrow$ LUMO+3) (99.6%) of same type LMCT for the  $\beta$ -spin. The second absorption band represented by the transitions HOMO-3 $\rightarrow$ LUMO (9.9%) for the  $\alpha$ -spin and HOMO-3 $\rightarrow$ LUMO+1 (81.3%) for the  $\beta$ -spin of the same character MLCT. The absorption spectra of the Co complex are the MLCT, LMCT and ILCT transfers.

The theoretical absorption spectrum of Ni complex shows two bands, the first intense band consists of two peaks located at 599 nm and 600 nm correspond to the transitions (HOMO-1 $\rightarrow$ LUMO + 3) (23.2%) for the  $\alpha$ -spin, (HOMO-1 $\rightarrow$ LUMO + 5) (62.0%) for the  $\beta$ -spin and (SOMO%LUMO + 3) (86.3%) for the  $\alpha$ -spin (HOMO-1 $\rightarrow$ LUMO + 5) (86.3%) for the  $\beta$ -spin of the same ILCT character for the four Transitions. The states calculated at 508 nm and 508 nm constitute the weak band, which gathers four main transitions (HOMO-1 $\rightarrow$ LUMO + 6) (13.1%) for the  $\alpha$ -spin, (HOMO-1 $\rightarrow$ LUMO + 9) (62.5%) for the  $\beta$ -spin and (HOMO-1 $\rightarrow$ LUMO + 7) (30.0%) for the  $\alpha$ -spin (SOMO $\rightarrow$ LUMO + 9) (32.3%) for the  $\beta$ -spin respectively of character ILCT (see **Figure S1**) (**Supplementary**).

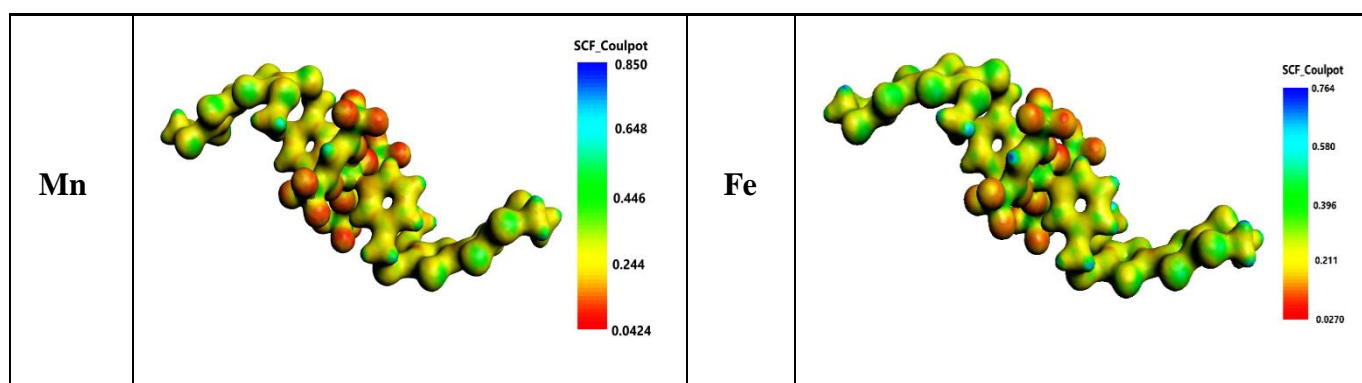
The Cu complex mainly presents three absorption band, the first located at 603 nm due to the transitions (SOMO $\rightarrow$ LUMO + 3), (HOMO-1 $\rightarrow$ LUMO + 2) for the  $\alpha$ -spin and HOMO-1 $\rightarrow$ LUMO + 4), (SOMO  $\rightarrow$ LUMO + 3) for the  $\beta$ -spin of the same ILCT character for the four Transitions, the second located at

592 nm constitutes three transitions corresponding to the same ILCT character since all the orbitals involved in these transitions are located on the ligand, the third peak calculated at 594 nm corresponds to a (HOMO-14→LUMO) (87.5%) transition with a charge transfer of metal-centered (MC) dominant character. The absorption spectrum of the Cu complex is mainly ILCT type.

The Zn complex shows five absorption bands of the same ILCT character, the first the most intense 387nm, corresponding to the transitions (HOMO-3→LUMO + 7) of nature (64.9%). The second located at 427nm correspond to the transitions (HOMO-2→LUMO + 3) (50.7%).the third absorption band presented the transition HOMO-1→LUMO+9 about 49.6%. the fourth less intense located at 549nm due to electronic transition from HOMO-1→ LUMO+7 (70.3%) .

### 1.6. Molecular electrostatic potential analysis (MEP)

To predict reactive sites for electrophilic or nucleophilic attack for the investigated molecules, the molecular electrostatic potential MEP has been calculated using the DFT- PBE/TZP. The MEPs surfaces of the compounds are shown in **Fig. 7**. It can be suggested that there are regions rich in electrons (deepest red) around the fluorine atoms F and the oxygen atoms of the hfac parts reflect the most electronegative region and have an excess of negative charge, subject to electrophilic attack. The green color surfaces over the carbon atoms characterizes a neutral region.



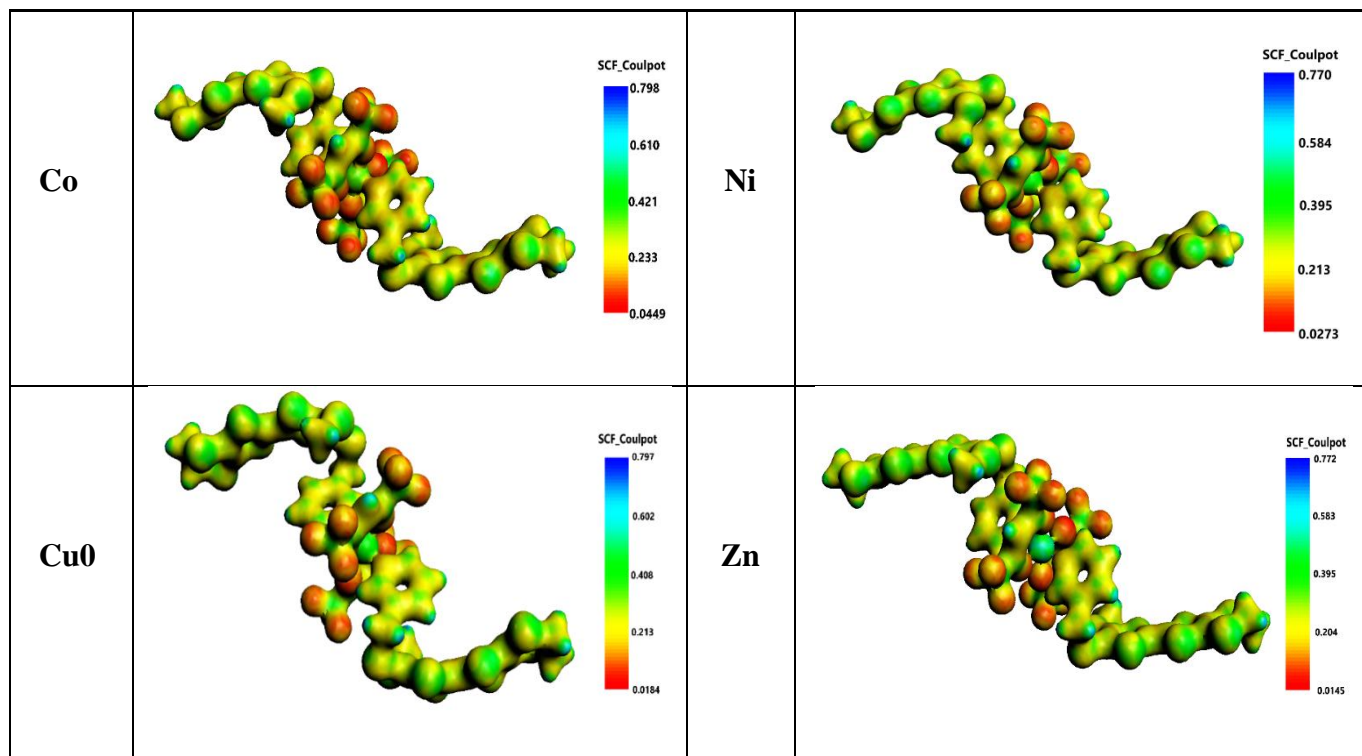


**Fig. 7** 3D molecular electrostatic potential (MEP) surfaces of  $M(\text{hfac})_2(\text{TTF})_2$ ] (where  $M = (\text{Mn (5), Fe (4), Co (3), Ni (2), Cu (1) and Zn (0))$ ).

The hydrogen atoms of the ligand part contain the positive electrostatic potential (blue regions), a zone subject to a nucleophilic attack. A partial negative charge covers the rest region of the TTF unit, establishing this region as subject to weak electrophilic attack. The yellow color is slightly inclined to the red color for the two compounds (Mn and Co). From **Fig. 7** understandably, the MEPs isosurfaces of designed molecules are almost similar. These results provide the necessary information about the possible reactive regions.

### 1.7. Non-Covalent Interaction (NCI)

To determine the positions and nature of the noncovalent interactions in the studied complexes, their NCI are visualized in 3D space, as shown in **Fig. 8**.

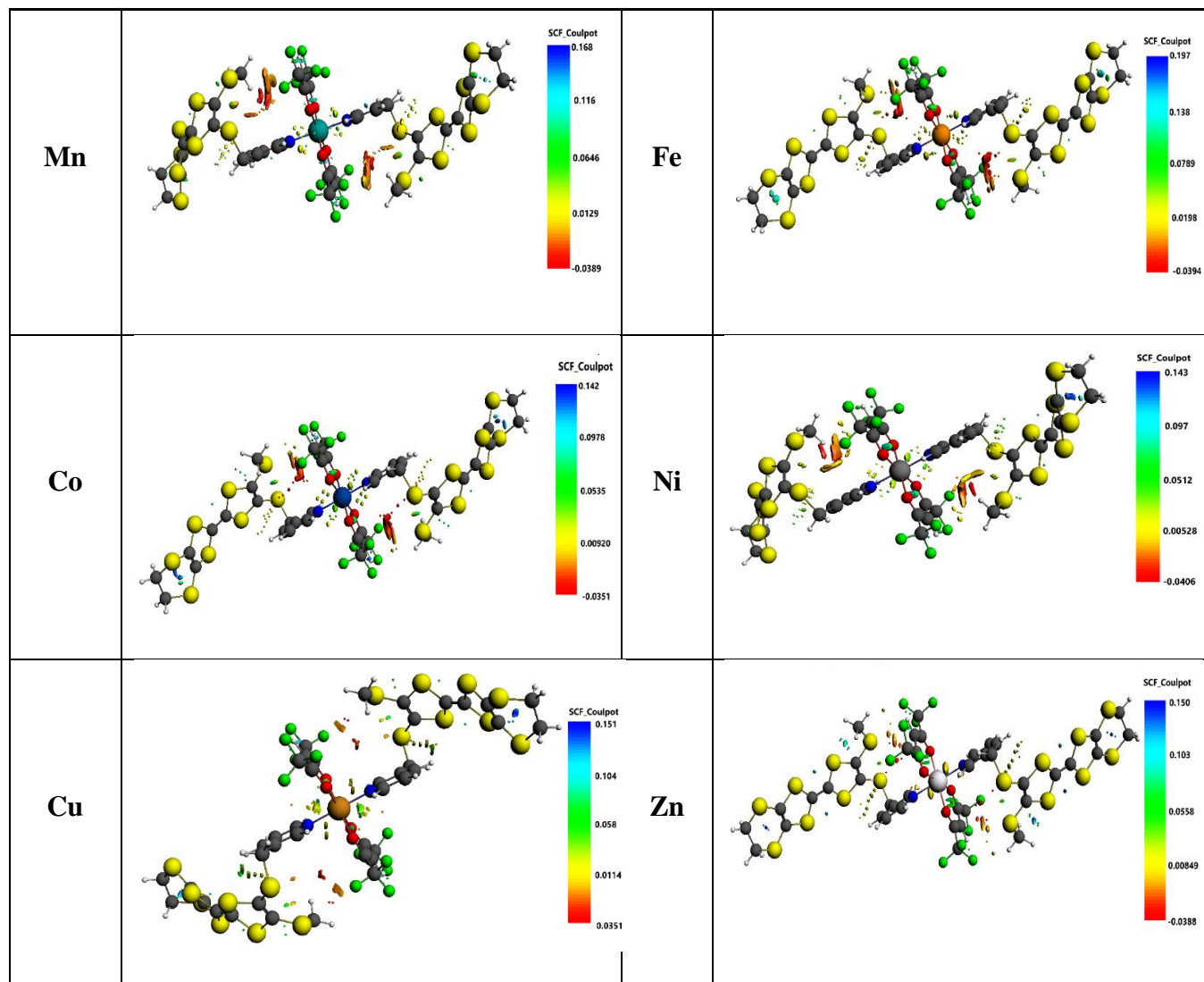


**Fig. 8** Three-dimensional NCI surfaces of  $[M(\text{hfac})_2(\text{TTF})_2]$  (where M= (Mn (5), Fe (4), Co (3), Ni (2), Cu (1) and Zn (0)).

As we observed through the NCI plots, greenish yellow isosurfaces are evidenced between the hydrogen (H) atoms of pyridine rings and the (S) of TTF unit indicating the existence of H-bondings.

The results show that the Zn and Cu complexes have weak repulsion contact between the fluorine and sulfur atoms. These later were represented by low percentage of yellow zones. However the other complexes (Mn, Fe, Co, Ni) have strong repulsive interactions (deep red).

In addition, the destabilized interactions (steric repulsion) are also observed as red color isosurfaces between S (5) and S(6) atoms in the ligand and the fluorine (F) and oxygen (O) atoms in the (hfac) part. A comparison of compounds studied reveals similar binding regions obtained from hydrogen and sulfur

bonding interactions. The relatively large contributions from the electrostatic interactions are reflected in the increase of spattered green regions. The steric repulsions decrease significantly for Cu and Zn, which exhibit diminutive red regions as shown in **Fig. 8**. These results highlight the existence of various types of weak interactions and show the agreement between AIM and NCI conclusions.

## 2. Molecular docking investigation

### 2.1. Computational details

It is known that tetrathiafulvalene ligands and complexes have two major biological activities: antifungal [39] and antibacterial [40]. To identify how our studied complexes  $M(\text{hfac})_2(\text{TTF})_2$  ( $M = \text{Mn, Fe, Co, Ni, Cu}$  and  $\text{Zn}$ ) could interact as antifungal and antibacterial agents, the molecular docking of the DFT-optimized complexes was performed against three related proteins taken from the Protein Data bank (<http://www.rcsb.org/pdb>): CYP121 (PDB: 2IJ7) [41] and CYP51 (PDB: 1EA1)[42] proteins were chosen as targets for antifungal activity evaluation in addition to

*E. coli* DNA gyrase B protein (PDB: 1KZN) [32] for antibacterial activity evaluation. The proteins were cleaned from water and freed from ligands (fluconazole and Clorobiocin) by Discovery Studio 3.5 Visualizer [33]. Then polar hydrogen atoms and Gasteiger charges were added to the proteins by using the AutoDockTools4 [34]. The molecular[43] docking was performed with deep learning by the means of GNINA 1.0 code [43] by choosing the “rescore” function based on convolutional neural networks (CNNs) scoring function. As the CNN score increases, the stability of the protein-ligand complex also improves. The GNINA algorithm is time consuming but gives better ligands ranking than AutoDock Vina scoring on redocking and cross-docking tasks [43]. **The molecular docking was performed for the studied complexes and native ligands** in the following search spaces (SS) and the box dimensions (BD): (PDB: 2IJ7; SS: X=10.69, Y=42.92, Z=134.01; BD: X=40, Y=40, Z=40), (PDB: 1KZN; SS: X= 19.53, Y = 19.50, Z = 43.03 ; BD: X=40, Y=40, Z=40) and (PDB: 1EA1; SS: X =-12.12, Y = -2.91, Z = 62.51; BD: X=40, Y=40, Z=40). The molecular docking protocol was validated by redocking using the published

crystal structures of protein–ligand complexes. The visualization of the results were depicted by Discovery Studio Visualizer software [6] [33].

## 2.2. Molecular Docking Results

Molecular docking became an important drug design tool to make new potent agents by investigating the binding pattern compounds toward target proteins. To identify how the studied ligands can bind to CYP121 (PDB: 2IJ7) and Cytochrome P450 14 alpha-sterol demethylase CYP51 (PDB: 1EA1) from *Mycobacterium tuberculosis* and *E. coli* DNA gyrase B protein (PDB : 1KZN) proteins. The complete molecular docking results of the studied complexes  $M(\text{hfac})_2(\text{TTF})_2$  (where: M = Mn, Fe, Co, Ni, Cu and Zn) i.e. CNN scores are listed in **Table 4**. It was found that the complexes Co/2IJ7, Zn/1EA1 and Co/1KZN show the best CNN scores, 0.2655, 0.3432 and 0.3862, respectively, as shown in **Fig. 9, 10** and **11** : An overview of the Protein–Complex binding surrounding interactions (a) interaction residues. Fig.9 depicts the 2IJ7 residues in interaction with Co: ARG95 and LYS105 by Hydrogen Bonding; PHE344, LYS100, ALA349, MET99 and LYS96 by hydrophobic interactions; ARG95, MET99, LYS96:NZ and PHE344 by other types of interactions. **Fig. 10** depicts the 1EA1 residues in interaction with Zn: ASN102 and GLY107 by Hydrogen Bonding; LEU301, ARG393, ALA398, ILE401 and LEU301 by hydrophobic interactions and LEU105 by other types of interactions. **Fig. 11** depicts the 1KZN residues in interaction with Co: ARG76 by Hydrogen Bonding; ALA53 and HIS116 by hydrophobic interactions with ASP49, GLU50, GLU50, ASP49 and HIS116 by other types of interactions.

Fluconazole, the native ligand for 1EA1, has a CNN score of 0.2935, indicating effective binding. The complex Zn0 has a slightly higher score of 0.3432, suggesting potentially stronger binding interactions compared to Fluconazole. For 1KZN, CBN, the native ligand, exhibits the highest CNN score of 0.3960, reflecting very strong binding. Co3opt shows a similar high score of 0.3862, indicating that it is a strong competitor. For 2IJ7, NAPD, the native ligand, has a CNN score of 0.3454, demonstrating effective binding. In comparison, Zn0 scores 0.2021, which is lower, suggesting weaker binding relative to NAPD.

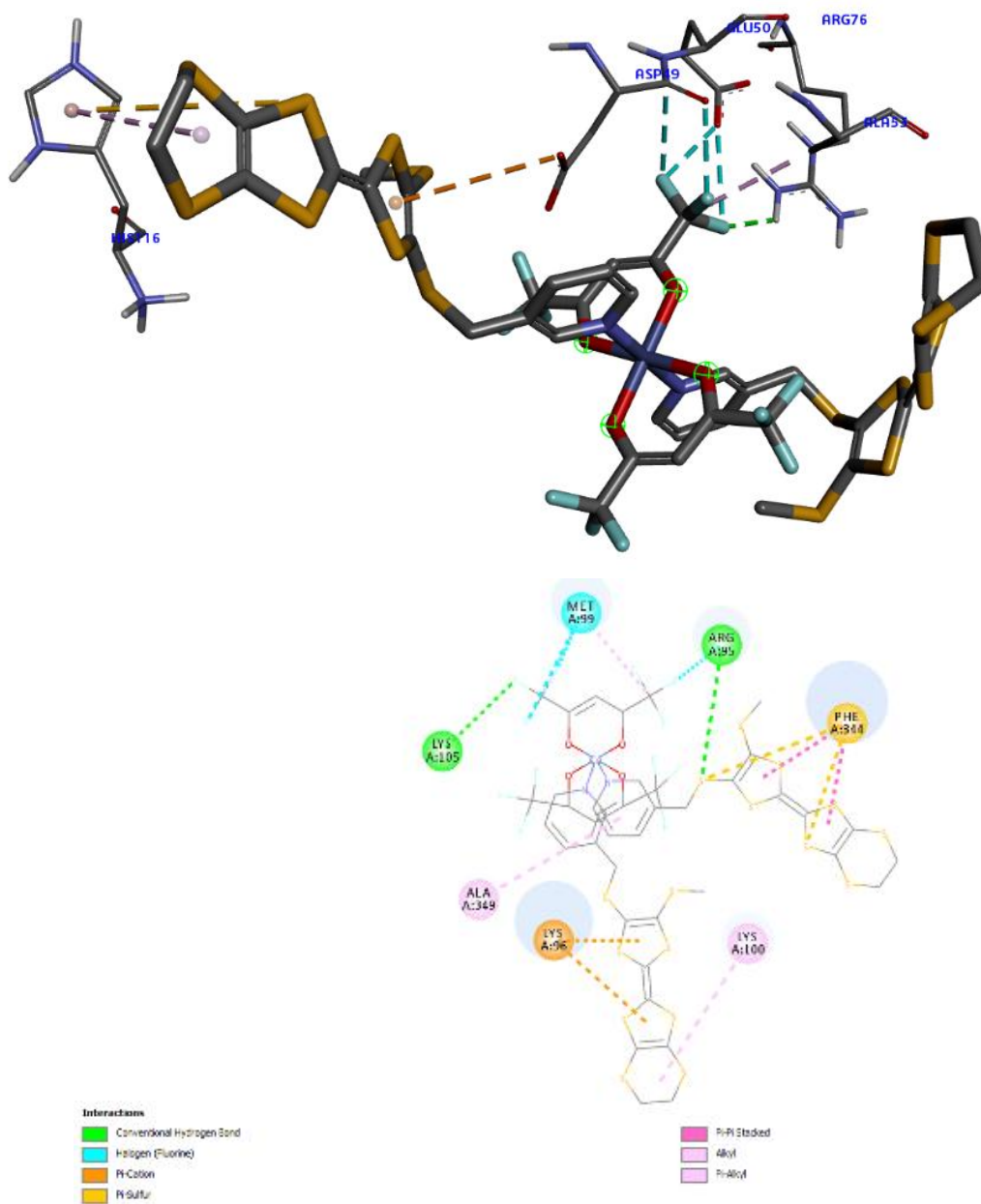


**Fig. 9** 2ij7/Co(3) complex

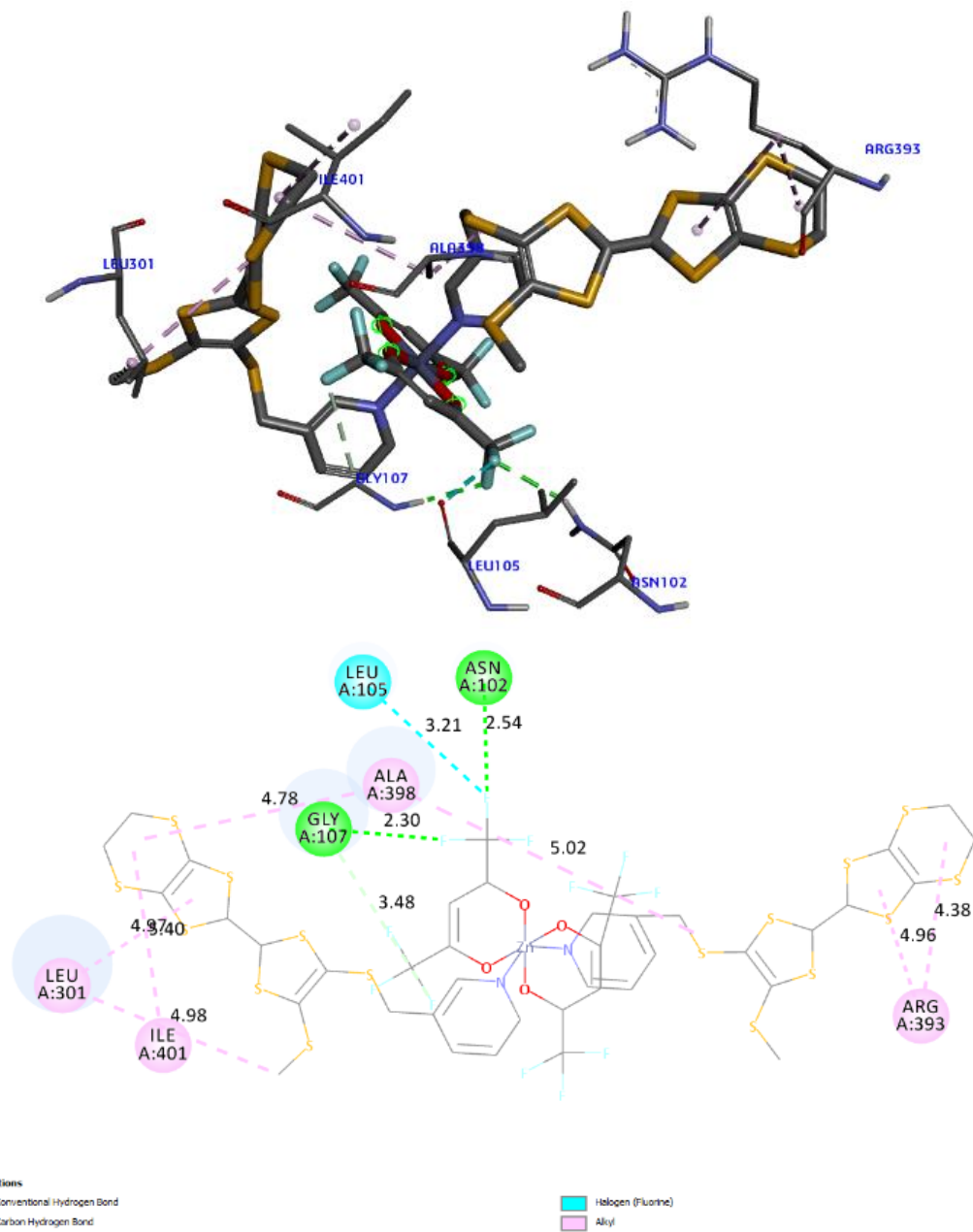


**Fig. 10** 1EA1/Zn (0) complex

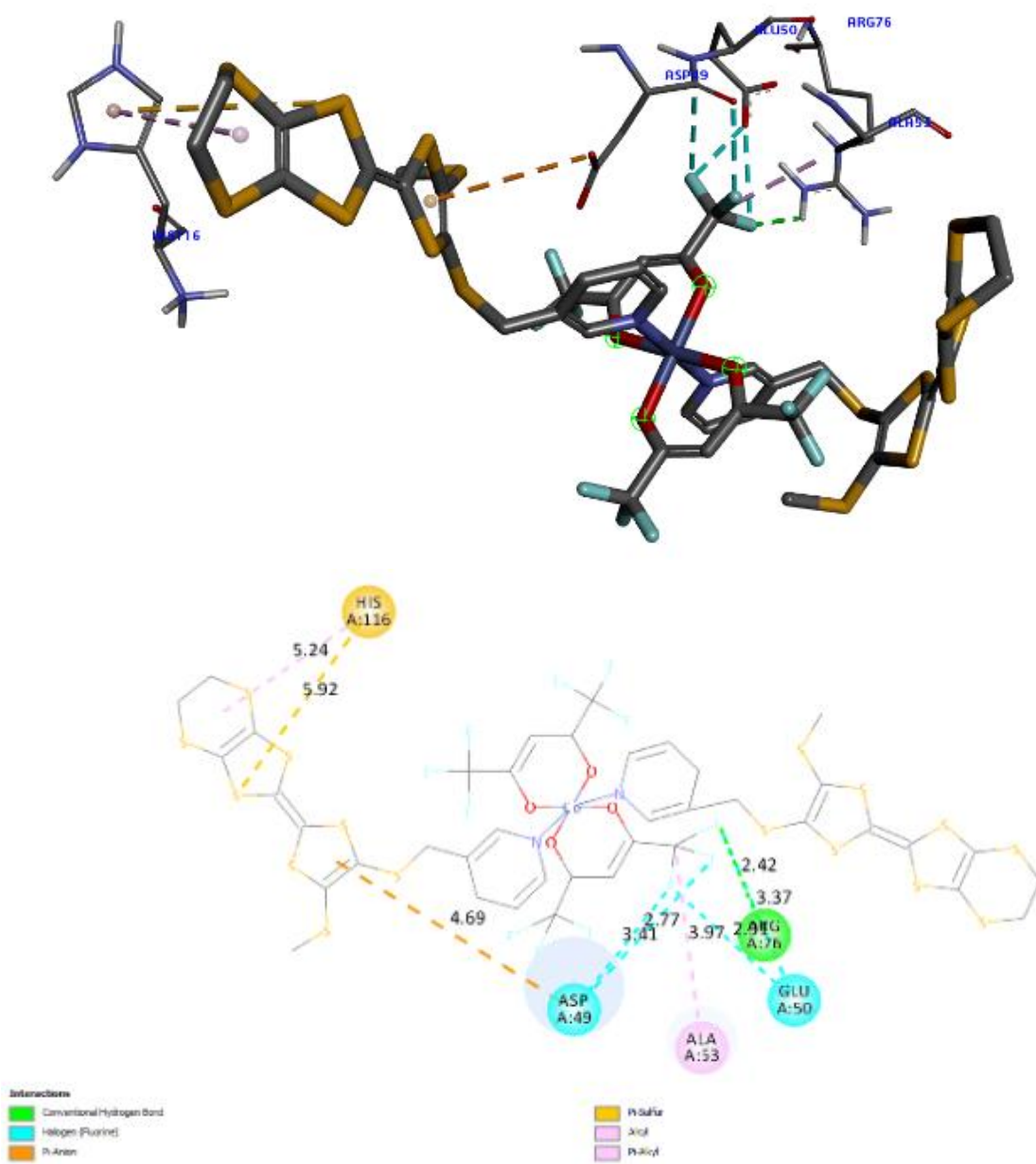


**Fig. 11** 1KZN/Co (3) complex

**Table 4.** CNN Scores for Studied Complexes and Native Ligands Binding to Targets 1ea1, 1KZN, and 2ij7

Compound	1ea1	1KZN	2ij7
Fluconazole	0.2935		
Clorobiocin		0.3960	
NAPD			0.3454
Zn (0)	0.3432	0.2044	0.2021
Cu (1)	0.2661	0.3778	0.2248
Ni (2)	0.2911	0.3547	0.2376
Co (3)	0.2478	0.3862	0.2655
Fe (4)	0.1092	0.2945	0.2258
Mn (5)	0.0709	0.2141	0.1573

## 4. Conclusion

In this article, a comparative study between a synthesized complex  $\text{Cu}(\text{hfac})_2(\text{TTF})_2$  and a series of homologous complexes has been reported with their electronic properties. Molecular geometries have been optimized with different spin states.

The most stable compounds (bonding energy) have the widest energy gap (maximum hardness principle) and a maximum spin multiplicity.

The small difference between the calculated total energies of different spin states, suggests the possibility of configuration changes. The complex with the Mn (0, 3) has the smallest energy gap (0.2 eV) so it is more conductive than the other compounds; which are rather semi-conductive with a gap of  $\sim 1$  eV.

Electronic population analysis of atomic orbitals 3d/4s in SOMO, HOMO/SOMO-1,-2 and -3 with different oxidation states 1+ and 12+ confirms that the copper is complexed into its ionic state.

TDDFT calculations show that the majority of transitions are of ILCT type for Ni, Cu and Zn complexes.

The use of AIM and NCI methods enabled us to look at the strength and type of interactions on the basis of electron density. The analysis of the topological parameters mainly suggests an electrostatic nature of most of the bonds. A high electron density value for M - N bonds proves that the latter are stronger than M-O bonds. This strength varies in the order  $\text{Zn} < \text{Ni} < \text{Mn} < \text{Fe} < \text{Co} < \text{Cu}$ . We also noted the existence of weak intramolecular hydrogen bonds  $\text{F} \cdots \text{H-C}$  and  $\text{S} \cdots \text{H}$ .

The results of molecular docking revealed that Zn and Cu could be potent antifungal agents in addition to Zn as antibacterial agent.

## Acknowledgments

The authors gratefully acknowledge the GENCI/CINES for HPC resources/computer time, through the project GENCI/IDRIS thanks to the grant AD010814932 on the supercomputer Jean Zay, and the PSMN of the ENS-Lyon for computing resources.

## ORCID

Samira ZEROUAL 0000-0003-2127-074X

Saliha BELHOUCHE 0009-0009-6357-6510

Saad BOUCHEKIOUA 0000-0001-7244-9614

Rafik MENACER 0000-0002-3742-8727

Noura BENBELLAT 0000-0003-4776-7770

Oussama KHAOUA 0000-0002-1514-8716

Henry CHERMETTE 0000-0002-5890-7479

## Bibliography

- [1] J. A. McCleverty and T. J. Meyer, *Comprehensive Coordination Chemistry II*, vol. 1–9. 2004. doi: 10.1016/C2009-1-28216-5.
- [2] S. T. Oyama, “Preparation and catalytic properties of transition metal carbides and nitrides,” *Catal. Today*, vol. 15, no. 2, 1992, doi: 10.1016/0920-5861(92)80175-M.
- [3] X. Y. Zhang, W. L. Yu, J. Zhao, B. Dong, C. G. Liu, and Y. M. Chai, “Recent development on self-supported transition metal-based catalysts for water electrolysis at large current density,” *Applied Materials Today*, vol. 22. 2021. doi: 10.1016/j.apmt.2020.100913.
- [4] M. V. Kurushkin, “Alfred Werner: Overlooked Genius of the Periodic System,” *Chemistry - A European Journal*, vol. 25, no. 69. 2019. doi: 10.1002/chem.201904321.
- [5] N. Benbellat, K. S. Gavrilenko, Y. L. Gal, O. Cador, S. Golhen, A. Gouasmia, J. M. Fabre, L. Ouahab., “Co(II)-Co(II) paddlewheel complex with a redox-active ligand derived from TTF,”

- Inorg. Chem., vol. 45, no. 26, 2006, doi: 10.1021/ic061680v.
- [6] N. Benbellat, Y. Le Gal, S. Golhen, A. Gouasmia, and L. Ouahab, "Synthesis, characterization and X-ray structures of tetrathiafulvalene-type electron donors bearing one pyridine group," *Synth. Met.*, vol. 162, no. 21–22, 2012, doi: 10.1016/j.synthmet.2012.08.018.
- [7] J. F. Wang, R. Y. Li, P. Li, and W. K. Dong, "Exploring coordination behaviors, structural characterizations and theoretical calculations of structurally different Cu(II), Co(II) and Ni(II) emissive complexes constructed from a salamo-based ligand and 4,4'-bipy," *Inorganica Chim. Acta*, vol. 518, 2021, doi: 10.1016/j.ica.2021.120247.
- [8] M. Manjunatha, V. Srinivasan, and S. Haseen Buvabi, "Biological studies of novel 22-Membered N<sub>2</sub>O<sub>2</sub> diazadioxa Macrocyclic Bis-Triazoles transition metal Complexes: Synthesis and physicochemical studies," *Mater. Today Proc.*, vol. 47, pp. 4538–4547, Jan. 2021, doi: 10.1016/J.MATPR.2021.05.422.
- [9] S. N. Sovari and F. Zobi, "Recent Studies on the Antimicrobial Activity of Transition Metal Complexes of Groups 6–12," *Chemistry (Switzerland)*, vol. 2, no. 2, 2020. doi: 10.3390/chemistry2020026.
- [10] R. Sharma, V. J. Singh, and P. A. Chawla, "Advancements in the Use of Platinum Complexes as Anticancer Agents," *Anticancer. Agents Med. Chem.*, vol. 22, no. 5, 2021, doi: 10.2174/1871520621666210805150705.
- [11] H. Akamatu, H. Inokuchi, and Y. Matsunaga, "Electrical conductivity of the perylene-bromine complex [6]," *Nature*, vol. 173, no. 4395, 1954. doi: 10.1038/173168a0.
- [12] D. S. Acker, R. J. Harder, W. R. Hertler, W. Mahler, L. R. Melby, R. E. Benson, W. E. Mochel., "7,7,8,8-Tetracyanoquinodimethane and its electrically conducting anion-radical derivatives," *Journal of the American Chemical Society*, vol. 82, no. 24, 1960. doi: 10.1021/ja01509a052.
- [13] F. Wudl, G. M. Smith, and E. J. Hufnagel, "Bis-1,3-dithiolium chloride: An unusually stable organic radical cation," *J. Chem. Soc. D Chem. Commun.*, no. 21, 1970, doi:

10.1039/C29700001453.

- [14] F. Wudl, D. Wobschall, and E. J. Hufnagel, "Electrical Conductivity by the Bis-1,3-dithiole-Bis-1,3-dithiolium System," *Journal of the American Chemical Society*, vol. 94, no. 2, 1972. doi: 10.1021/ja00757a079.
- [15] J. Ferraris, D. O. Cowan, V. Walatka, and J. H. Perlstein, "Electron Transfer in a New Highly Conducting Donor-Acceptor Complex," *J. Am. Chem. Soc.*, vol. 95, no. 3, 1973, doi: 10.1021/ja00784a066.
- [16] R. Mayer and B. Gebhardt, "Schwefel- Heterocyclen und Vorstufen, XXXIII. Präparative Synthese und Folgereaktionen des Isotrithions (1.3- Dithiol- thions- (2)) und Isodithions (1.3- Dithiol- ons- (2))," *Chem. Ber.*, vol. 97, no. 5, 1964, doi: 10.1002/cber.19640970513.
- [17] H. Prinzbach, H. Berger, and A. Lüttringhaus, "Protonenaktivität im 1.3-Dithiolium-System," *Angew. Chemie*, vol. 77, no. 10, 1965, doi: 10.1002/ange.19650771007.
- [18] D. S. Acker and W. R. Hertler, "Substituted Quinodimethans. I. Preparation and Chemistry of 7, 7, 8, 8-Tetracyano Quino Dimethan," *J. Am. Chem. Soc.*, vol. 84, no. 17, 1962, doi: 10.1021/ja00876a028.
- [19] S. Etemad, T. Penney, E. M. Engler, B. A. Scott, and P. E. Seiden, "Dc Conductivity in an Isostructural Family of Organic Metals," *Phys. Rev. Lett.*, vol. 34, no. 12, 1975, doi: 10.1103/PhysRevLett.34.741.
- [20] A. N. Bloch, D. O. Cowan, K. Bechgaard, R. E. Pyle, R. H. Banks, and T. O. Poehler, "Low-temperature metallic behavior and resistance minimum in a new quasi one-dimensional organic conductor," *Phys. Rev. Lett.*, vol. 34, no. 25, 1975, doi: 10.1103/PhysRevLett.34.1561.
- [21] C. S. Jacobsen, K. Mortensen, J. R. Andersen, and K. Bechgaard, "Transport properties of some derivatives of tetrathiafulvalene-tetracyano-p-quinodimethane (TTF-TCNQ)," *Phys. Rev. B*, vol. 18, no. 2, 1978, doi: 10.1103/PhysRevB.18.905.
- [22] A. Miyazaki et al., "Weak ferromagnetism of (BDH-TTP)[M (isoq)<sup>2</sup> (NCS)<sup>4</sup>](M= Cr, Fe; isoq=

- isoquinoline),” *Synth. Met.*, vol. 137, no. 1–3, pp. 1195–1196, 2003.
- [23] S. Belhouchat, S. Zeroual, N. Benbellat, O. Khaoua, S. Bouchekioua, R. Menacer, H. Chermette., “DFT and Docking Calculations of the Structural, Electronic, Biological and Conductivity Properties of the Synthetic Complex [Cu (hfac) 2 (L) 2][PF6] 2,” *ChemistrySelect*, vol. 9, no. 1, p. e202304155, 2024.
- [24] E. Van Lenthe, E. J. Baerends, and J. G. Snijders, “Relativistic total energy using regular approximations,” *J. Chem. Phys.*, vol. 101, no. 11, 1994, doi: 10.1063/1.467943.
- [25] S. com, “Search—Amsterdam Modeling Suite: Making Computational Chemistry Work for You Software for Chemistry & Materials”.
- [26] J. P. Perdew, S. H. Vosko, Koblar A. Jackson, Mark R. Pederson, D. J. Singh, C. Fiolhais et al., “Atoms, molecules, solids, and surfaces: Applications of the generalized gradient approximation for exchange and correlation,” *Phys. Rev. B*, vol. 46, no. 11, 1992, doi: 10.1103/PhysRevB.46.6671.
- [27] N. Huu Tho, T. T. Tu, T. M. Nhan, P. H. Cam, and P. T. Thi, “The Geometries and Stabilities of Neutral and Anionic Vanadium Doped Germanium Clusters VGen0/-( n = 9 - 13): Density Functional Theory Investigations,” *VNU J. Sci. Nat. Sci. Technol.*, vol. 35, no. 1, 2019, doi: 10.25073/2588-1140/vnunst.4827.
- [28] R. F. W. Bader, “A Quantum Theory of Molecular Structure and Its Applications,” *Chem. Rev.*, vol. 91, no. 5, 1991, doi: 10.1021/cr00005a013.
- [29] K. M., “program DGrid, Version 4, 2008”.
- [30] G. Scalmani, M. J. Frisch, B. Mennucci, J. Tomasi, R. Cammi, and V. Barone, “Geometries and properties of excited states in the gas phase and in solution: Theory and application of a time-dependent density functional theory polarizable continuum model,” *J. Chem. Phys.*, vol. 124, no. 9, 2006, doi: 10.1063/1.2173258.
- [31] X. L., V. Madison, A. S. Chau, D. Loebenberg, R. E. Palermo, P. M. McNicholas., “Three-

Dimensional Models of Wild-Type and Mutated Forms of Cytochrome P450 14 $\alpha$ -Sterol Demethylases from *Aspergillus fumigatus* and *Candida albicans* Provide Insights into Posaconazole Binding,” *Antimicrob. Agents Chemother.*, vol. 48, no. 2, 2004.

- [32] D. Lafitte, V. Lamour, P. O. Tsvetkov, A. A. Makarov, M. Klich, P. Deprez, D. Moras, C. Briand, R. Gilli., “DNA gyrase interaction with coumarin-based inhibitors: The role of the hydroxybenzoate isopentenyl moiety and the 5'-methyl group of the noviose,” *Biochemistry*, vol. 41, no. 23, 2002, doi: 10.1021/bi0159837.
- [33] “Discovery Studio Visualiser.” BIOVIA, Dassault Systèmes, 2005.
- [34] G. M. Morris, H. Ruth, W. Lindstrom, M. F. Sanner, R. K. Belew, D. S. Goodsell, A. J. Olson., “Software news and updates AutoDock4 and AutoDockTools4: Automated docking with selective receptor flexibility,” *J. Comput. Chem.*, vol. 30, no. 16, 2009, doi: 10.1002/jcc.21256.
- [35] O. Trott and A. J. Olson, “AutoDock Vina: Improving the speed and accuracy of docking with a new scoring function, efficient optimization, and multithreading,” *J. Comput. Chem.*, vol. 31, no. 2, 2010, doi: 10.1002/jcc.21334.
- [36] R. D. Shannon, “Revised effective ionic radii and systematic studies of interatomic distances in halides and chalcogenides,” *Acta Crystallogr. Sect. A*, vol. 32, no. 5, 1976, doi: 10.1107/S0567739476001551.
- [37] M. Souto *et al.*, “A highly stable and hierarchical tetrathiafulvalene-based metal-organic framework with improved performance as a solid catalyst,” *Chem. Sci.*, vol. 9, no. 9, 2018, doi: 10.1039/c7sc04829g.
- [38] “Solid State Physics. Von N. W. Ashcroft und N. D. Mermin; Holt, Rinehart and Winston, New York 1976, XXII, 826 Seiten, \$19,95,” *Phys. unserer Zeit*, vol. 9, no. 1, 1978, doi: 10.1002/piuz.19780090109.
- [39] T. Abbaz, A. Bendjeddou, A. Gouassmia, D. Bouchouk, C. Boualleg, N. Kaouachi, N. Inguibert, D. Villmin., “Synthesis, Characterization and Antibacterial Activity of Cyclic Sulfamide Linked to

- Tetrathiafulvalene (TTF),” *Lett. Org. Chem.*, vol. 11, no. 1, 2014, doi: 10.2174/157017861101140113162502.
- [40] A. Ayadi, A. Jaafar, A. Fix-Tailler, G. Ibrahim, G. Larcher, and A. El-Ghayoury, “Tetrathiafulvalene based electroactive ligands and complexes: Synthesis, crystal structures and antifungal activity,” *Tetrahedron*, vol. 73, no. 25, 2017, doi: 10.1016/j.tet.2017.05.046.
- [41] H. E. Seward, A. Roujeinikova, K. J. McLean, A. W. Munro, and D. Leys, “Crystal structure of the Mycobacterium tuberculosis P450 CYP121-fluconazole complex reveals new azole drug-P450 binding mode,” *J. Biol. Chem.*, vol. 281, no. 51, 2006, doi: 10.1074/jbc.M607665200.
- [42] L. M. Podust, T. L. Poulos, and M. R. Waterman, “Crystal structure of cytochrome P450 14 $\alpha$ -sterol demethylase (CYP51) from Mycobacterium tuberculosis in complex with azole inhibitors,” *Proc. Natl. Acad. Sci.*, vol. 98, no. 6, pp. 3068–3073, 2001.
- [43] A. T. McNutt, P. Francoeur, R. Aggarwal, T. Masuda, R. Meli, M. Ragoza, J. Sunseri, D. R. Koes., “GNINA 1.0: molecular docking with deep learning,” *J. Cheminform.*, vol. 13, no. 1, 2021, doi: 10.1186/s13321-021-00522-2.